EARTHQUAKE PERFORMANCE OF AUSTRIAN DAM, CALIFORNIA DURING THE LOMA PRIETA EARTHQUAKE

By John Vrymoed [1], Wallace Lam[2]

Abstract

Austrian Dam is a 180-foot high embankment dam which was severely damaged during the October 17, 1989 Loma Prieta Earthquake. It was fortuitous that the reservoir was nearly empty at the time as the dam experienced significant cracking and deformations. Observation of the locations of cracking and the response of piezometers led to an understanding of an embankment dam's failure mode. Based on this understanding, the materials' undrained shear strength characteristics were used to predict deformations and pore pressures using both a non-linear decoupled and a fully coupled non-linear analysis. This case history demonstrated the threat that transverse cracking and adverse soil-structure interaction pose to safe performance during significant earthquake shaking.

Purpose

The California Division of Safety of Dams has initiated a comprehensive independent review of case histories of dams subjected to strong earthquake motion. Analyses are conducted on those cases where sufficient data are available. This review will afford a better understanding of performance as well as test out soil and mathematical models which will aid the Division's program to assess the seismic performance of dams in the State's highly seismic regions. Austrian Dam, presented here, is an example of one important case history. Upper San Fernando Dam, another important case history, is presented in a companion paper in these conference proceedings.

Austrian Dam Location and Embankment Properties

Austrian Dam is located within California's Santa Cruz Mountains in an area of high seismicity. The dam is situated at the convergence of the Sargent Fault located 700 feet northeast of the dam, and the San Andreas Fault approximately 1700 feet southeast of the dam. Built in 1951, the dam is 180 feet high, has 15 feet of freeboard and impounds a 6200 acre-foot reservoir. The dam's foundation is a thin-bedded clay shale while the abutments are comprised of a Franciscan sandstone and clay shale. Both the up and downstream slopes are 2.5:1 near the crest and transition to 3.5:1 near the toes. The dam's maximum cross-section and location of

[1] Chief, Design Engineering Branch, Division of Safety of Dams, Department of Water Resources, CA
[2] Senior Engineer, Design Engineering Branch, Division of Safety of Dams, Department of Water Resources, CA

piezometers are shown in Figure 1.

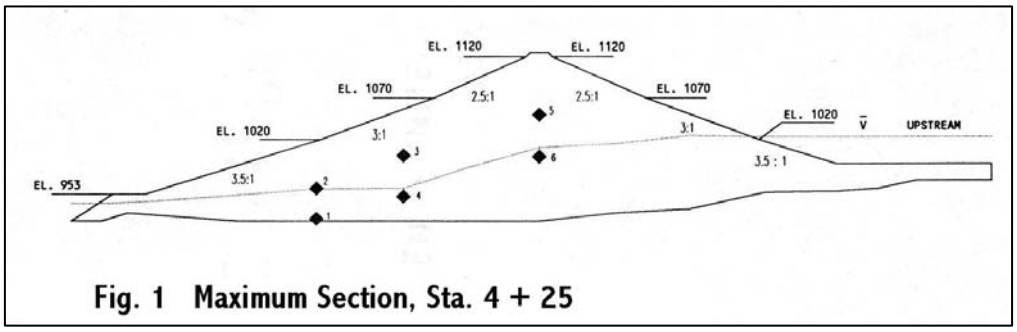

Fig. 1 Maximum Section, Sta. 4 + 25

The dam is a rolled earthfill and is nearly homogeneous. An attempt was made during construction to place the more impervious materials in the upstream zone. The average percent passing the #200 sieve for up and downstream zones are 25 and 18 percent, respectively. Other average in-situ material properties are as follows: water content, 12%; liquid limit, 32%; plasticity index, 15%; dry density, 127 lbs/ft3; Unified Soil Classification, GC-SC; maximum dry density, 128.4 lbs/ft3 at a moisture content of 10.3 percent which is equivalent to 99 percent relative compaction. The latter was based on ASTM 1557-79 modified to include 1 inch material and a compactive energy of 20,000 ft-lbs/ft3.

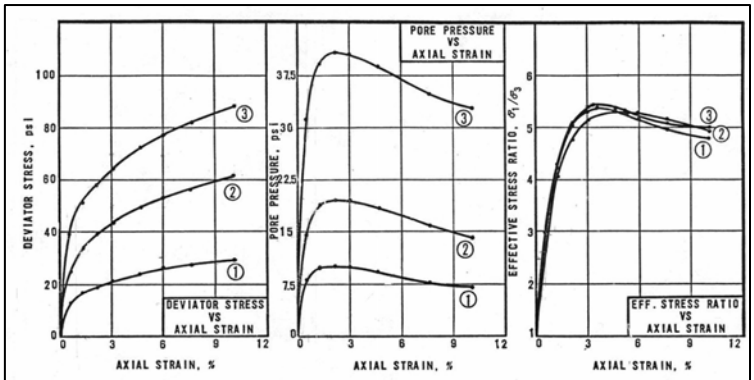

Fig. 2 Stress, Strain & Pore Pressure Relationships

Isotropically consolidated undrained triaxial (ICUE) tests with pore pressure measurements were carried out on six 5.75-inch diameter undisturbed samples taken from both the up and downstream zones. Results for three tests are shown in Figure 2. Test results showed no significant difference in strength characteristics between the material from the up and downstream zones. Combining all test results, average effective strength values of 44 degrees friction and zero cohesion and total strength values of 21 degrees friction and 290 lbs/ft2 cohesion were determined. The foregoing properties were determined by Wahler Associates in a 1979 seismic stability investigation.

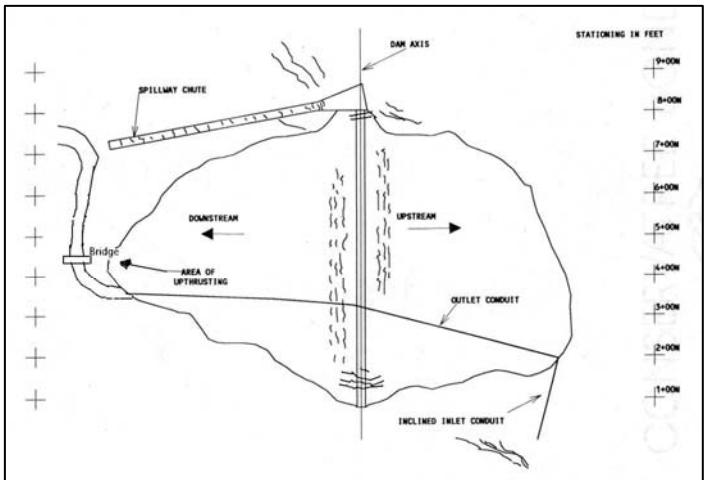

Fig. 3 Locations of Cracking and Deformations

Earthquake Damage

The epicenter of the main shock of the October 17, 1989 Loma Prieta earthquake was sited approximately 7 miles south of Austrian Dam. There were no accelerometers on or in close proximity to the dam to record ground motions. The Corralitos station, which recorded a peak ground acceleration of 0.64g, was approximately 5 miles east of the epicenter. The ground motions recorded at the Corralitos station are assumed to be an approximation of the motions experienced at the dam site because of the similarity of epicentral distances. The Division is currently conducting research to predict ground motions at the dam site based on current tectonic models of the region.

The plan view of Austrian Dam with the earthquake induced cracking is shown in Figure 3. The cracking and movement are categorized as follows: 1. down slope movement of the right abutment causing severe damage to the spillway in the form of tension cracks along its entire length; 2. significant cracking and displacement at the embankment and spillway wall contact at the right abutment; 3. down slope movement of the left abutment near the sloping intake tower in the form of shallow surface sliding; 4. 60-foot wide zones of parallel cracks on both the up and downstream slopes parallel to and below the crest; 5. upthrusting at the downstream toe; 6. through going en-echelon transverse cracking of the crest near the left abutment to a depth of 32 ft.

There was significant evidence of compression and upthrusting at the downstream toe. A bridge located near the toe was moved off its foundation and displaced downstream 18 inches. Any evidence of upthrusting at the upstream toe was concealed by the reservoir. There was no evidence of cracking on the crest other than the transverse cracking near the abutments. Neither was there any evidence of cracking below the zones of parallel cracking on either slope near the crest.

Dam Crest Survey Monuments

Vertical and horizontal crest displacements have been monitored since construction of the dam with 14 survey monuments located at 50-foot intervals along the crest. The vertical and horizontal displacements before and after the earthquake are shown in Figure 4. In this figure, Sta. 0+00 corresponds to a point near the left abutment while Sta. 7+50 corresponds to a point near the spillway entrance at the right abutment.

Prior to the earthquake, the last two readings were taken on September 15, 1989, and October 16, 1989, one day

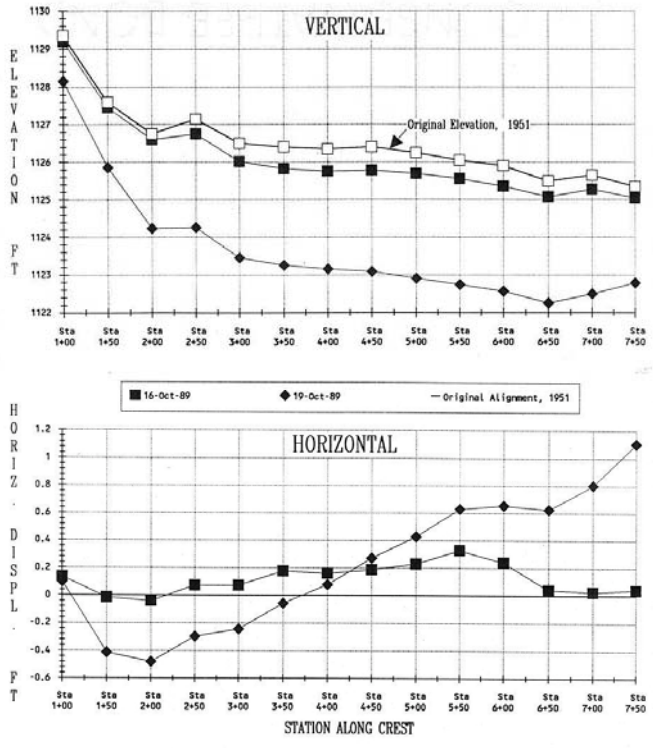

Fig. 4 Crest Deformations

before the earthquake. A reading was taken the day after the earthquake on October 18, 1989. Subsequent readings over a period of 19 days did not indicate any additional displacements.

The largest vertical displacement was 2.8 feet. Starting from Sta. 1+00 at the right abutment, the horizontal displacements were in an upstream direction up to Sta. 3+60. From there, the horizontal displacement reverses direction indicating a net downstream displacement. The large downstream displacements of the last two stations near the spillway were attributed to sliding of the right abutment. Except for these, the earthquake induced displacements are an amplification of the historic displacement due to the static stress conditions since the dam's construction.

Piezometer Readings

Six piezometers were installed in 3 holes as part of the 1979 seismic stability investigation. The piezometer installations consisted of porous stone/tubing encapsulated in 5 feet of sand and separated from one another with a plug of bentonite pellets.

Piezometer readings before and after the earthquake, as well as the increase in head and the corresponding pore pressure ratio, are shown in Table I. Fortunately, like the crest monuments, the piezometers were read the day before and were reread two days after the earthquake. Readings of piezometers 3 and 5 showed them to be dry. The readings for #6 and #4 showed a gradual decay of 20 and 10 feet, respectively over a period of 10 days. Hence, the pressures increases were probably higher immediately after the earthquake. The pore pressure increases took months to decay. The reservoir elevation was Elev. 1023.5 at the time of the earthquake.

Table I Piezometer Elevations, Increases and Ratios

Piezometer	Tip Elev	Oct.16 Elev	Oct.19 Elev	Increase	PP Ratio
1	923	960	1015	55	0.29
2	960	968	977	9	0.1
3	1000	dry	dry	0	0
4	950	960	973	13+	0.07+
5	1050	dry	dry	0	0
6	999	1012	1062	50+	0.18+

Mode of Failure - Field Observations

The mode of failure became clear when the presence, as well as absence, of longitudinal cracking below the crest were examined. The locations of longitudinal cracking were superimposed on three cross-sections taken perpendicular to the crest at stations 2+50, 4+25, and 6+00 as shown in Figure 5. Also shown are the corresponding vertical and horizontal measured crest displacements. The phreatic surface measured at Sta. 4+25 just before the earthquake has been superimposed on the other two cross-sections. Also shown in Figure 5 is the postulated mode of failure of deep seated shearing within a shear zone. In this mode of failure the longitudinal cracking on one side

of the crest is associated with movement of the block above a shear zone on the opposite side of the crest.

Sta. 6+00 The embankment at Sta. 6+00, which is near the right abutment, is postulated to have experienced deep seated shearing in both directions. This resulted in upstream displacement due to shearing through the saturated portion of the upstream embankment fill and downstream displacement due to instability of the materials forming the right abutment.

The right abutment had experienced slide failures during construction and had historically undergone minor movements. The latter was evidenced by stained hairline cracks on the spillway walls. The stability of the right abutment prior to the earthquake was therefore marginal. As a result, the earthquake caused the hillside forming the right abutment above the spillway to move downward causing scarps up to 3 feet in depth.

The horizontal crest displacements between Sta. 6+00 and the spillway were therefore heavily influenced by displacement of the right abutment. This can be seen on Figure 4 which shows the horizontal displacements increasing dramatically when the right abutment contact is approached. This is accompanied by lesser amounts of longitudinal cracking on the downstream face. As a result, movement in a downstream direction dominated, causing a net horizontal crest displacement of 0.4 feet.

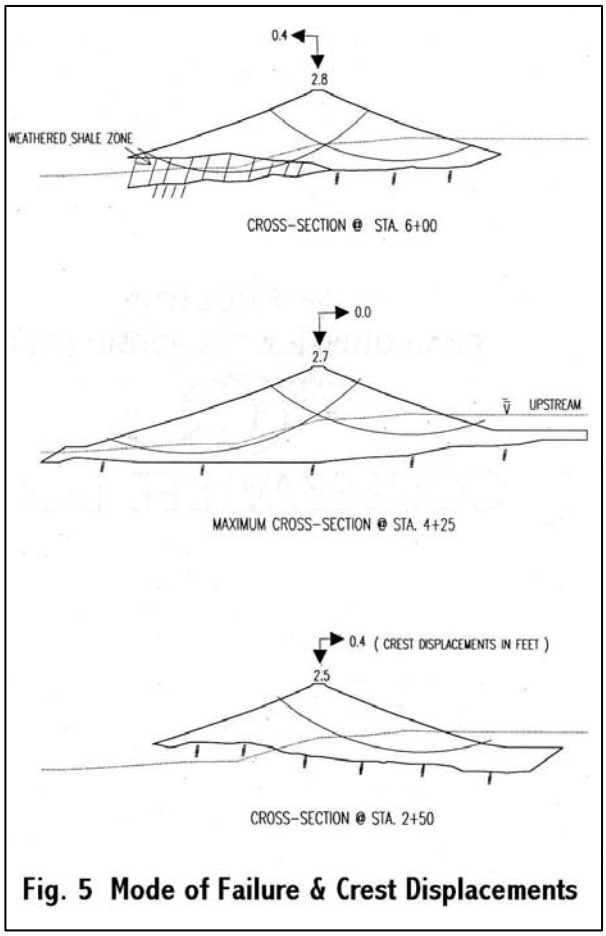

Fig. 5 Mode of Failure & Crest Displacements

Sta. 4+25 The cross-section at Sta. 4+25 represents the maximum section. The embankment at this station is symmetrical except for a slight rise in the elevations of the upstream foundation contact and phreatic surface. Because of the near symmetry, the horizontal displacements, as a result of deep seated shearing, canceled one another. A vertical displacement of 2.6 feet was measured at this station.

Sta. 2+50 The cross-section at Sta. 2+50 is near the left abutment. At this location there was deep seated shearing in only the upstream direction. The abutment upstream of the crest near the sloping intake tower showed evidence of shallow sliding. The sloping intake tower was examined and no signs of distress or damage were found. The 48-inch outlet conduit was examined on the inside throughout its entire length and was similarly found to have suffered no distress. This was evidenced by the absence of any cracking of its mortar lining. Hence, deep seated sliding of the abutment upstream of the crest was ruled out and the sliding that did occur was concluded to have been shallow and to not

have affected or contributed to the deep seated shearing of the upstream embankment materials.

The abutment downstream of the crest showed no evidence of movement. The downstream embankment material at this station was above the phreatic surface which inhibited deep seated shearing from occurring. As a result, there was no associated longitudinal cracking on the upstream face. Starting from Sta. 1+00, longitudinal cracking on the upstream face can be seen to begin at Sta. 3+75, which is where the downstream embankment material first becomes saturated.

The possibility of lateral spreading or settlement by shallow surface sliding was investigated by noting the longitudinal cracking on the downstream face at Sta. 2+50. If this cracking was as a result of shallow sliding then the crest displacement should have been in a downstream direction. Instead, the displacement was in an upstream direction.

Trenching done in areas of longitudinal cracking on both the up and downstream faces of the dam showed all cracks to be normal to the slope. The cracks typically dipped from 77 to 82 degrees with the horizontal and extended to a depth of 6 to 10 feet before pinching out. These angles match the angle of resultant displacement of 81 degrees determined by combining the horizontal and vertical displacements at Sta. 2+50. This computation is possible at this station because there was no downstream displacement to offset the upstream crest displacement.

The inclination of the cracking further discounts shallow surface sliding and supports the postulated deep seated shearing. Hence, a mode of failure of lateral spreading whereby the longitudinal cracking represents scarps as a result of shallow sliding or settlement was ruled out.

Indirect evidence of a shear zone was noted by the difficulty experienced in lowering a water measuring probe in the tubing for piezometers #1 and #6. For piezometer #1 the tubing was significantly deformed between Elevations 955 and 960 which corresponds to an elevation of 25 to 30 feet above the bedrock contact; while the tubing for piezometer #6 was deformed between Elevations 1040 and 1017 which is directly below the crest at mid-height.

The only plausible mode of failure is deep seated shearing. In this mode of failure, the up and downstream portions of the embankment slide as a result of shearing through a defined zone. The wedge forming the crest also behaves as a rigid block and acts like a graben with respect to the slopes. This indicates that, during high levels of acceleration, the embankment can no longer act as a continuum as the slopes act independently of one another.

Non-Linear Decoupled Analysis

Based on the foregoing field observations, a decoupled analysis was conducted whereby the downstream zone of the maximum

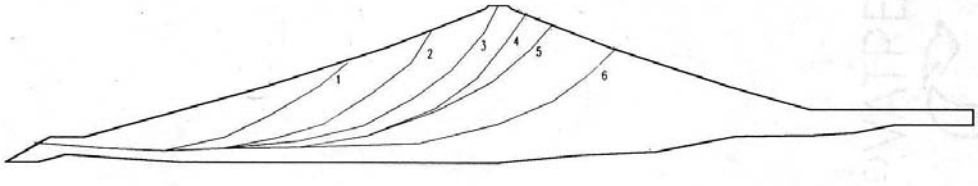

Fig. 6 Location of Critical Failure Surface

cross-section was analyzed to determine if a slope stability analysis could predict the location of longitudinal cracking. Six failure surfaces, shown in Figure 6, having the same coordinates near the toe, were varied throughout the downstream zone so that the slopes on either side of the crest were intersected at different locations. Results indicated that failure surface #4, intersecting upstream zone below the crest, was the most critical. This location coincides with the location of longitudinal cracking on the upstream slope. Hence, the earthquake induced cracking occurred at the location were mobilization of static stresses are predicted to be maximized.

In slope stability analyses it is common to represent a failure surface by a single plane. This is adequate for estimating safety factors determined by comparisons of resisting and driving forces or of available and mobilized strengths. In a computation of displacements, however, the extent over which they occur cannot be ignored. Displacements, after all, are a result of strains which are due to an applied stress. Hence, if displacements are to be computed, the zone over which they occur has to be quantified.

Zones of longitudinal cracking are commonly observed on the surface of fills where an embankment is rapidly loaded either statically or dynamically. The extent of these zones can be estimated by performing slope stability analysis. Typically, critical failure surfaces whose safety factors vary by approximately 5 percent, tend to be concentrated in a defined zone as was the case for Austrian Dam. In the analysis, the extent of the shear zone was based on the measured extent of longitudinal cracking of 60 feet on both faces of the dam. It was assumed that this thickness remains constant along the zone's entire length. The deformation of the piezometer tubing suggested that this is a reasonable assumption.

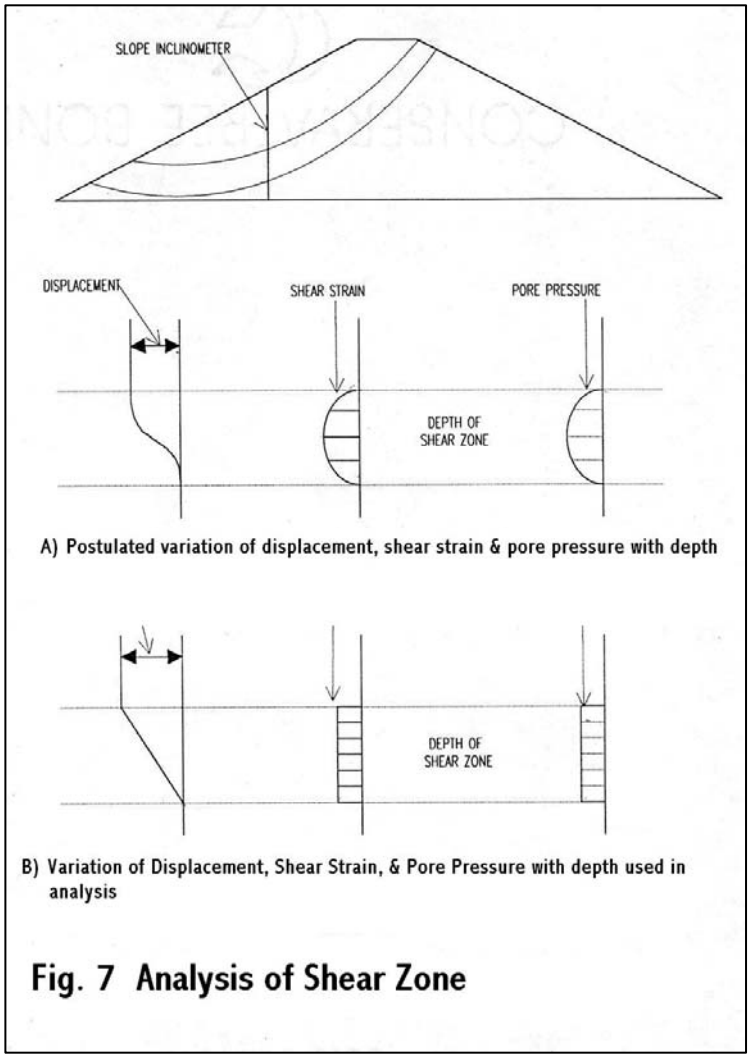

A) Postulated variation of displacement, shear strain & pore pressure with depth

B) Variation of Displacement, Shear Strain, & Pore Pressure with depth used in analysis

Fig. 7 Analysis of Shear Zone

Displacements are computed by analyzing the shear zone to determine its effect on the yield acceleration of the block above it. The analysis considers a plane strain condition where the soil is sheared over the thickness of the shear zone as illustrated in Figure 7. Figure 7a shows the postulated variation of permanent displacement with depth as measured by a hypothetical slope inclinometer and the

corresponding shear strains and pore pressures. To simplify the analysis, a linear variation of displacement was assumed which results in constant average shear strains and pore pressures as shown in Figure 7b.

Yield Function

In a determination of displacements, Newmark's method is often used whereby the acceleration time history is integrated using a constant yield acceleration. In this analysis, Newmark's method is also used because this method is observed to capture the failure mode characterized by blocks sliding due to inertia forces. A refinement is introduced whereby the yield acceleration is varied to account for the shear strength mobilized at varying levels of strain and displacement – the latter determined by applying the strain over the extent of the shear zone. This variation of yield acceleration is referred to as a yield function and is established by determining the shear strength parameters by digitizing the applicable stress strain curves. Ideally, anisotropically consolidated strength data would be used. In this analysis, ICUE strength data were used to determine the yield function as these were the only data available. The resultant yield functions are shown in Figure 8 for a reservoir level existing at the time of the earthquake and a full reservoir.

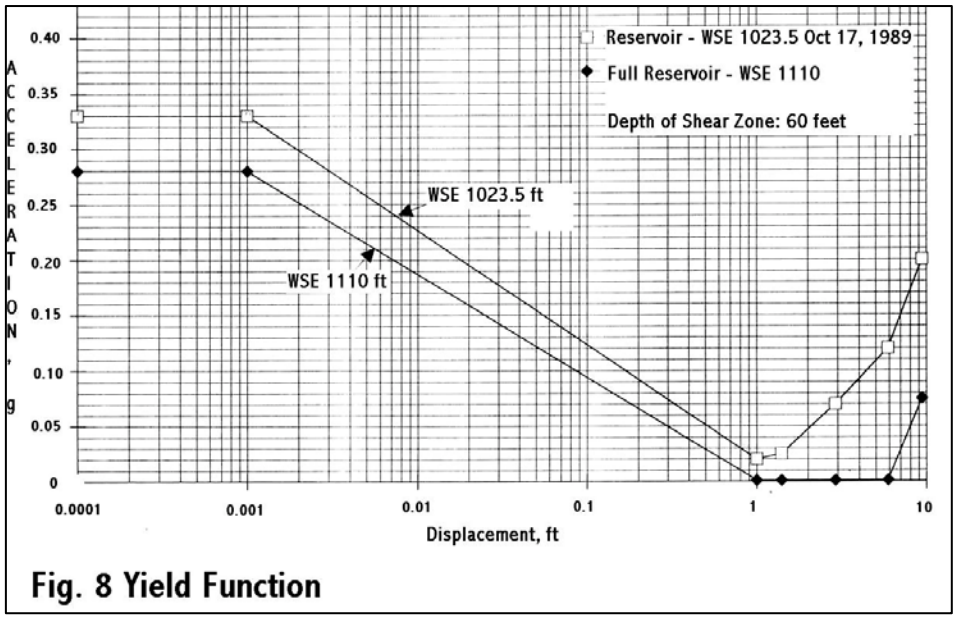

Fig. 8 Yield Function

Although the shear strength increases with an increase in strain, the yield function's variation of yield acceleration with displacement is mostly reflective of the pore pressures induced during shear. Starting with zero pore pressure at the threshold acceleration, the pore pressures gradually increase with increasing displacements which results in a decrease in the yield acceleration. For the Austrian Dam materials, the lowest yield acceleration closely corresponds to displacements/strains which are associated with maximum pore pressures. Then, as the induced strain increases further, the yield acceleration increases as the pore pressure gradually decreases. The steps taken to develop a yield function are provided in detail in Appendix I.

The yield functions for the up and downstream shear zones at the time of the earthquake were found to be nearly identical which is reflective of the similarity between the strengths and showed the differences in elevations of the phreatic surface and bedrock contact to be negligible.

Computed Displacements

Having determined the yield function for both the up and downstream zones for Sta. 4+25, the maximum cross section, the permanent displacements were determined by double integration of the Corralitos acceleration time history using a time step of 0.02 seconds.

The acceleration time history is shown in Figure 9 with the corresponding yield acceleration superimposed. Also shown are the computed displacements and pore water pressure ratios. The pore pressure ratio is the pressure normalized with the initial effective confining pressure from the ICUE tests. It represents the effect of undrained shearing on the average pore pressure within the shear zone. Yield functions were similarly calculated for Sta. 2+50 which is near the left abutment and displacements calculated. The resultant displacements are shown in Table II.

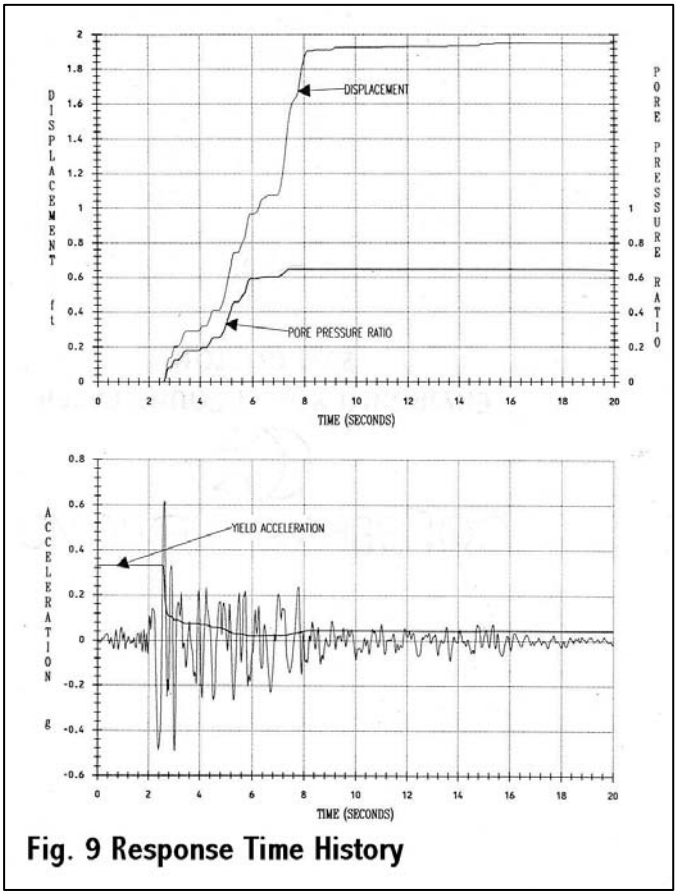

Fig. 9 Response Time History

The displacements in Table II represent the movement of the blocks above the up and downstream shear zones. These displacements are representative of shear strains on the order of 3.3 percent. To determine displacement of the crest, the displacement of these blocks were combined vectorially, as shown in Table III, using an angle with the horizontal of 81 degrees. This angle was measured in the field and also corresponds to the angle between the vertical and horizontal displacements measured at Station 2+50.

Table II Computed Block Displacements

Block	Sta. 4+25	Sta. 2+50
Upstream	1.95	2.12
Downstream	1.95	0.06

TABLE III Crest Displacements in feet, negative values = upstream

	Sta. 4+25		Sta. 2+50	
Displacement	Calculated	Measured	Calculated	Measured
Vertical	3.8	2.6	2.1	2.5
Horizontal	0.0	0.0	-0.3	-0.4

A computation of crest displacements for the cross-section at Sta. 6+00 was not carried out due to the unknown strength of the weathered shale overlying the bedrock downstream of the crest. Exploration subsequent to the earthquake determined the weathered shale to be 68 ft. in depth in this area of the embankment. Since the strength of this material is unknown, any computation of displacement is speculative. However, the performance of the right abutment suggests that the weathered shale has a lower strength than the embankment materials. As a result, the net measured displacement in a downstream direction would be predicted.

A crest displacement of 8.2 ft. was determined using the yield function representing a full reservoir. This amount of displacement was in the range of displacements predicted in the 1979 seismic stability investigation. However, the design input motion used in that investigation was 10 times more severe, having 60 seconds of significant shaking compared to the 6 seconds of the Corralitos record.

Pore Pressures

Pore pressures are predicted based on the pressures generated during undrained shear at strains equivalent to those computed in the analysis. The analysis determined a displacement of 2 feet which, averaged over the 60-foot wide shear zone, results in a shear strain of 3.3 percent. This shear strain equates to approximately 2.3 percent axial strain in a lab sample. Ideally, this strain would be used to predict the pore pressures generated during shear in an anisotropically consolidated test (ACUE) because this test appropriately accounts for zero pore pressure at the initial stress condition of a slope prior to the earthquake. Because no samples were tested under these conditions, the ICUE generated pore pressures have to be reduced to account for the anisotropic stress conditions in the field.

The appropriate strain values and corresponding pore pressures used to make this reduction are explained in Appendix II. Accounting for anisotropy, the calculated average pore pressure ratio of 0.18 is very close to the observed average of 0.16. The range of observed ratios is from 0.07+ to 0.29 as indicated in Table I.

Fully Coupled Non-Linear Analysis

A fully coupled nonlinear dynamic analysis was performed using finite difference computer code FLAC 2D, (5.0 version 346, Itasca) for purposes of comparing deformations and shear strains determined from the foregoing decoupled analysis. The strain-hardening/softening (SS) plastic model, one of the built-in constitutive models in FLAC, was utilized to define the plastic deformation and strength behavior of the embankment soils. The SS model is based on the Mohr-Coulomb plasticity model which allows the user to define the shear strength parameters as piece-wise linear functions of shear strain.

Similar to the decoupled analysis, the embankment materials' drained and undrained shear strengths were represented by values of friction angle and cohesion based on the ICUE stress-strain curves shown in Figure 2. The average K_{2max} value of 120, used for assigning the shear modulus, was based on the resonant column tests performed in the 1980s (Reference 7). Hysteretic damping was applied to the model

elements corresponding to the modulus reduction and damping ratio curves for sandy soils used in SHAKE. A small amount of Rayleigh damping was added at the nodes to damp out any high frequencies. The free-field is applied on the side boundaries and the seismic loading, input as a shear stress wave, was assigned to the boundary.

Dynamic Response

The maximum cross-section at STA. 4+25 was modeled with the reservoir elevation and phreatic surface at the time of the earthquake. Areas of shear strain concentration are shown Figure 11, which indicates distinct bands of averaging approximately 3 percent. This shear strain is equivalent to that calculated in the decoupled analysis and is slightly greater than the 2.7 percent back calculated from field measurements.

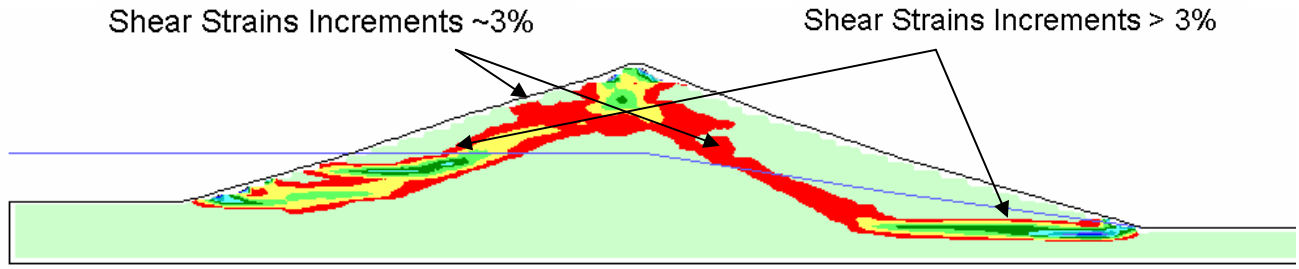

Figure 11: Shear Strain Increments during LPEQ Shaking

The earthquake-induced displacements of the upstream and downstream slopes, shown in Figure 12, can be characterized as blocks moving in opposite directions. The displacement vectors gradually diminished with depth indicating the lower center portion of the embankment was not affected by the earthquake.

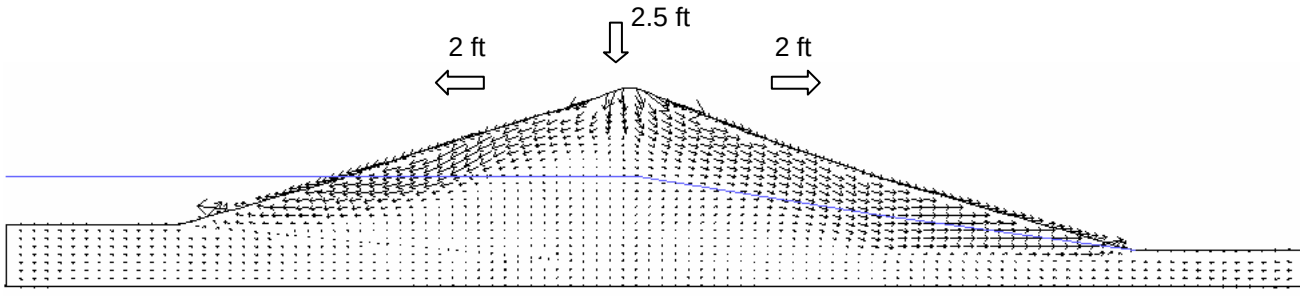

Figure 12: Displacement Vectors

The up and downstream blocks intersect near the crest, resulting in an average vertical deformation of 2.5 ft in the upper 20 ft of the embankment. The analysis also predicts compression bulges at both toes.

Lateral displacements and shear strains were plotted with depth, shown in Figure 13, at a vertical alignment through the downstream slope, connecting piezometers P1 and P2, approximately two thirds of the way down the slope. The plots are shown at different points in time during the earthquake. Also shown on this Figure is the location where the

piezometer tubing was bent which is shown to be coincident at a depth where the shear strains dramatically increase.

The FLAC predicted shear strains and displacements, shown in Figure 13, are similar to those postulated in the decoupled analysis, shown in Figure 7. FLAC predicts the extent of shearing to occur over a depth of 45 feet which is less than the 60 feet observed on the extent of longitudinal cracking on the slopes. It also predicts the extent of shearing, at depth, to increase during the earthquake time history. The resultant displacement of the downstream block is about 2 feet which is equal to the computed displacements at Sta. 4+25 as shown in Tables II and III.

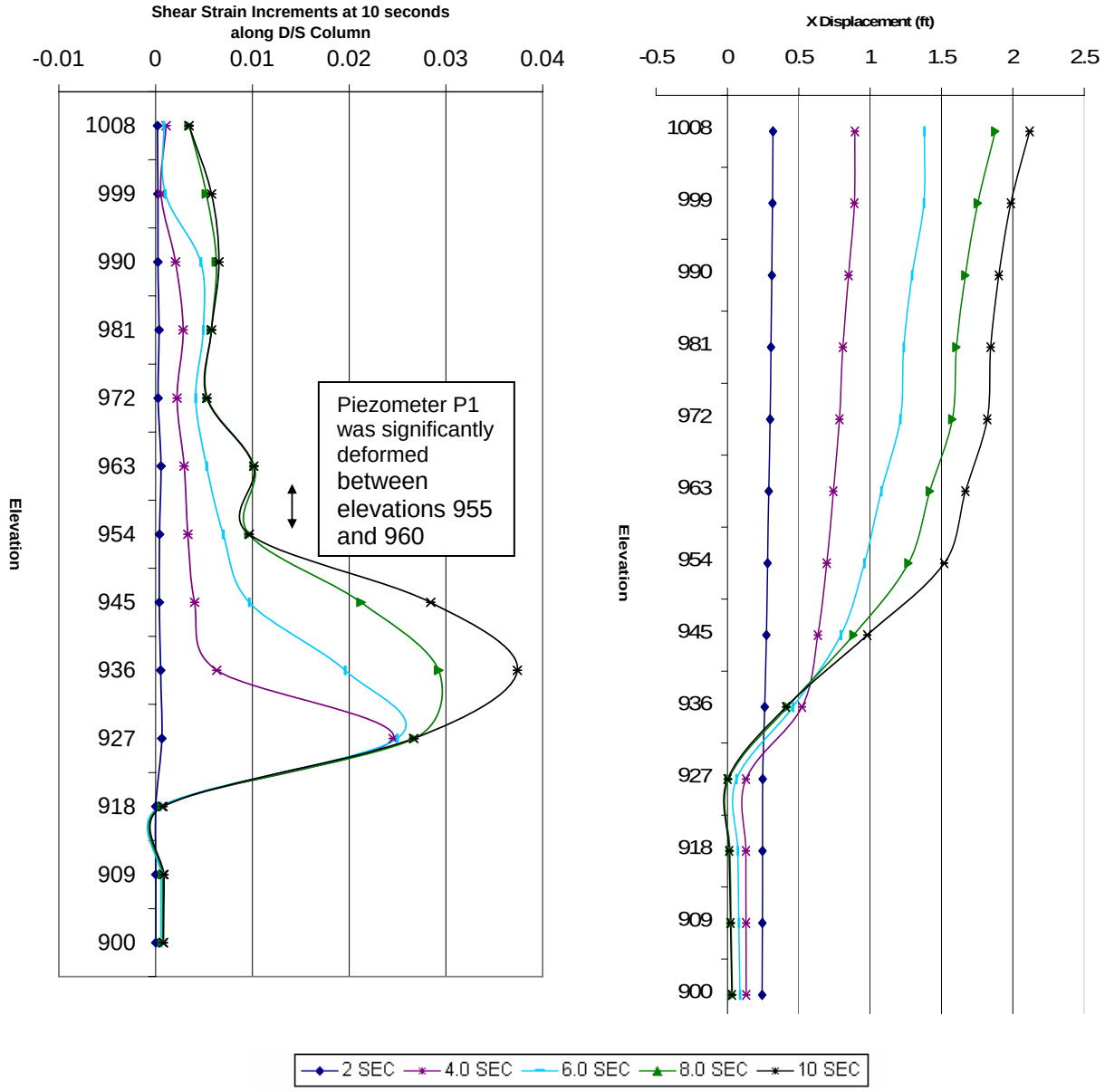

Figure 13: Displacement/ Shear Strains Vertical Profiles – Downstream Slope

Deformations and Transverse Cracking

In a typical seismic safety evaluation, as was done in the 1979 investigation, the estimated deformations were compared to the available freeboard. All too often, if the deformations are judged to be within the available freeboard, the dam is judged safe. The case history of Austrian Dam points out the necessity of evaluating the attendant consequence of deformations on any soil structure interaction and transverse cracking. Also, soil strengths are typically taken at strains of 5 or 10 percent to determine safety factors or displacements. As the foregoing analysis indicates, a strain of 2 percent can result in very significant deformations and associated cracking.

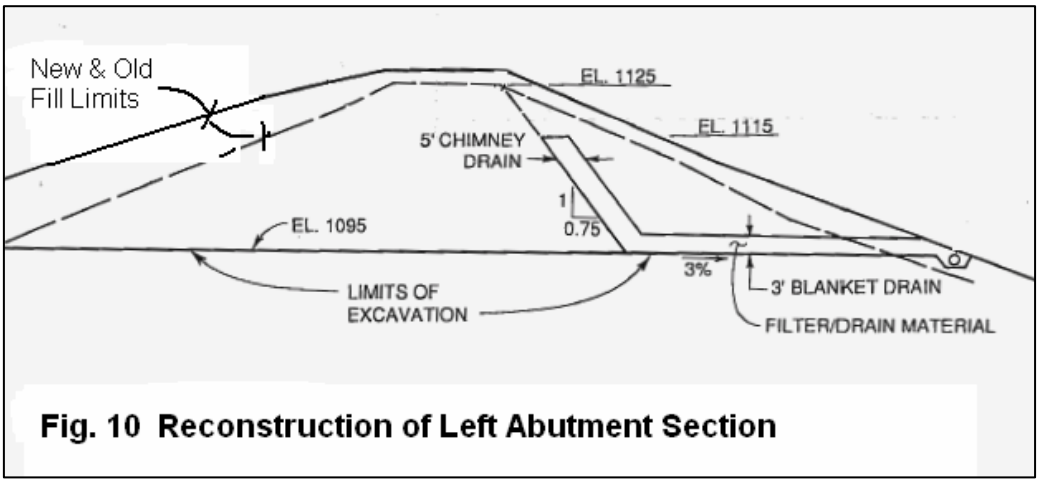

Fig. 10 Reconstruction of Left Abutment Section

The displacements experienced by Austrian Dam demonstrated the potential for an uncontrolled release by either, cracking at the spillway wall/embankment contact, and/or the transverse cracking. The latter was found to extent to a depth of 32 feet – more than twice the available freeboard. The repairs that were undertaken would not have been possible with a full reservoir. The spillway, which was severely damaged, was quickly repaired in preparation of the fall rainy season and a new spillway subsequently constructed on the opposite abutment. The upper portion of the embankment was excavated at both abutments and reconstructed with internal drainage as a mitigation measure against transverse cracking, as shown in Figure 10.

Summary and Conclusions

Careful examination of the performance of Austrian Dam during the 1989 Loma Prieta Earthquake afforded an understanding of an embankment's mode of failure during strong shaking. This mode of failure can be characterized as deep seated shearing where the embankment behaves as distinct blocks. The movements of these blocks are governed by inertia forces and the undrained strength characteristics of the materials.

As predicted, shearing will occur where the materials' static strengths are mobilized to their greatest extent. As a result, the pattern of deformation occurring statically over time is a precursor to the pattern of earthquake induced deformation. Understanding the mode of failure allows for both a non-linear decoupled and coupled analysis. Both analyses provide nearly identical results given the same undrained strength characteristics and input motion. The resultant shear strains, displacements and pore pressures closely correspond to those measured. The validity of comparing computed

values with those measured is tempered by the fact that the former are based on the use of the Corralitos time history which was recorded some distance away from the dam. The California Division of Safety of Dams has initiated program to generate synthetic time histories at the site using the latest available seismological models of the area in an effort to develop this case history to the maximum extent possible.

The significant dam safety lesson that this case history taught is that soil structure interaction and transverse cracking are highly probable modes of failure. Hence, it was fortuitous that the reservoir level was as low as it was at the time of the earthquake.

APPENDIX I YIELD FUNCTION DETERMINATION

1. Determine the width of shear zone based on either or in combination of the following:
   A. Field performance
   B. Slope stability analyses
   C. Mathematical models such as FLAC
2. Determine the threshold acceleration at 0.001 ft of displacement
   A. Find the elastic/plastic yield point from undrained shear strength relationships. For ICUE tests, for medium dense to dense soils, this typically occurs at 1percent axial strain, and approximately 0.5 percent for loose soils.
   B. Determine the threshold yield acceleration using the effective strengths corresponding to the yield point. Accelerations less than threshold do not result in displacement or pore pressures as the embankment is predicted to respond as an elastic continuum.
3. Determine the yield acceleration values at strain values equal to and greater than the yield point.
   A. Determine the total strength values corresponding to values of the yield point and greater and use these to determine the respective yield acceleration.
   B. The corresponding displacements are determined by taking the axial strain values, multiplying these by (1+poisson's ratio), and applying the latter over the shear zone.

APPENDIX II CONVERSION OF ICUE PORE PRESSURES TO ACUE CONDITIONS.

The values in parentheses represent the values obtained from the data used in the analysis.

1. Determine the principal effective stress ratio from slope stability analysis for the static, pre-earthquake condition, (2.7)
2. Find the corresponding axial strain and pore pressure ratio from ICUE test, see Figure 2 (0.5%, 0.52)
3. Determine the shear strain from field observations if possible, otherwise use slope stability analyses; take one half the vertical displacement at Sta. 4+25 - this equals one slope's displacement taken over 60 feet (2.3%)
4. Convert this shear strain to a corresponding ICUE axial strain, axial strain= shear strain/(1+poisson's ratio) (1.7%)
5. Combine this axial strain with the axial strain from Step #2, (2.2%)
6. Find the pore pressure ratio which corresponds to this combined axial strain from the ICUE tests, see Fig. 2 (0.7)
7. The ACUE pore pressure is the pore pressure in Step #6 minus the pore pressure in Step #2 (0.18)

APPENDIX III REFERENCES

1. Boutrup, E., "Computerized Slope Stability Analysis For Indiana Highways," Joint Highway Research Project, Report No. 77-25, School of Civil Engineering, Purdue University.

2. Division of Mines and Geology, "Plots of the Processed Data for the Interim Set of 14 Records from the Santa Cruz Mountains (Loma Prieta) Earthquake of October 17, 1989," Department of Conservation, State of California, Office of Strong Motion Studies, December 13, 1989.

3. Newmark, N.M., "Effects of Earthquakes on Dams and Embankments," Geotechnique, Volume 15, Number 2, June 1965.

4. Rodda, K.V., Pardini, R.J., "Remedial Construction of Austrian Dam Following the Loma Prieta Earthquake," Issue No. 92, USCOLD Newsletter, July 1990.

5. Seigel, R.A.," Computer Analysis of General Slope Stability Problems," Joint Highway Research Project Report No. 75-8, School of Civil Engineering, Purdue University.

6. Wahler Associates, "Initial Evaluation of Seismic Stability of Austrian Dam, December, 1979," File No. 622-13, Item No. 8, California Department of Water Resources, Division of Safety of Dams.

7. Wahler Associates, "Seismic Safety Evaluation of Austrian Dam For San Jose Water Works, August 1981," File No. 622-13, Item No. 10, California Department of Water Resources, Division of Safety of Dams.

8. Wahler Associates, "Austrian Dam, Investigation and Remedial Construction Following the October 17, 1989 Loma Prieta Earthquake," Volume I-Text, Division of Safety of Dams File No. 622-13, Item #11.